Density Functional Theory for Magnetism and Magnetic Anisotropy

Gustav Bihlmayer

Contents

Abstract

Density functional theory and its application for the simulation of magnetic properties of condensed matter is introduced. This includes vector-spin density functional theory for the evaluation of spin-spin interactions and relativistic extensions to capture effects like the magnetocrystalline anisotropy. The role of the different approximations to the exchange-correlation functional, e.g., the local density approximation, or the generalized gradient approximation, is investigated, showing successes and limitations of the present functionals. Special techniques to determine, e.g., the magnetic ground state or finite temperature properties based on density functional theory are shortly discussed.

G. Bihlmayer (✉)
Peter Grünberg Institut and Institute for Advanced Simulation, Forschungszentrum Jülich and JARA, Jülich, Germany
e-mail: g.bihlmayer@fz-juelich.de

W. Andreoni, S. Yip (eds.), *Handbook of Materials Modeling*,
https://doi.org/10.1007/978-3-319-42913-7_73-1

1 Introduction

Being a material-specific theory, density functional theory (DFT) has gained enormous popularity in the last few decades for the investigation of structural, electronic, or optical properties of condensed matter and is valued as 'approximate practical method' in many other areas as well (Jones 2015). In the field of magnetism the value of DFT calculations is widely accepted: only few input parameters have to be known (the chemical composition and, maybe, some information on the crystal structure) to calculate ground state properties like the magnetic order (ferro- or antiferromagnetic, non-collinear structures etc.), spin- and orbital magnetic moments, magnetic interaction parameters (e.g., the spin-stiffness), or the easy axis (or plane) of magnetization. These 'ab-initio' parameters can further be used to determine properties beyond the ground state, for example spin-wave spectra or ordering temperatures. In many cases, the results are of excellent quality, in particular in the field of itinerant magnets DFT results usually have predictive power.

To illustrate these statements, magnetic moments and ordering temperatures of several Co-based Heusler compounds are compiled in Table 1 (Thoene et al. 2009). The structure of these compounds consists of four interpenetrating face-centered cubic (fcc) lattices where the atoms of the formula Co_2YZ are located. Here, Y is another transition metal element, while Z is from the p-block of the main group. The DFT calculations give access not only to the total magnetic moment in the unit cell, M_{tot}, which is in good agreement with the experimental values, but also to locally resolved quantities. E.g., one can see a considerable variation of the Co moments for the listed Co_2YZ structures, depending on their neighboring atoms. With increasing total moment also the Curie-temperatures rises in the shown series, a trend that is also confirmed experimentally.

Despite the many successes of DFT in the field of magnetism, one has to be aware of possible complications that can arise due to the specific nature of some materials. This can be e.g., correlation effects that are difficult to capture in DFT calculations (Galler et al. 2015) or zero-point fluctuations that have to be accounted for (Ibañez Azpiroz et al. 2016). However, also in these cases DFT can be used as a starting point to explore the magnetic properties of materials.

All specific examples shown in this chapter are bulk magnets that can be reliably calculated with different basis sets, e.g., planewaves, augmented plane

Table 1 Magnetic moment, M, in μ_{B} per site (Co or Y) or unit cell (tot) and Curie temperature (T_{C}, in Kelvin) of several Heusler compounds: The moments and exchange interactions were obtained in DFT, while T_{C} is calculated from these DFT results in the mean-field approximation. Experimental values are listed for comparison. (From Thoene and coworkers 2009)

Co_2YZ	$M_{\mathrm{Co}}^{\mathrm{calc}}$	M_{Y}^{calc}	$M_{\mathrm{tot}}^{\mathrm{calc}}$	$M_{\mathrm{tot}}^{\mathrm{exp}}$	$T_{\mathrm{C}}^{\mathrm{calc}}$	$T_{\mathrm{C}}^{\mathrm{exp}}$
Co_2TiAl	0.48	−0.08	0.85	0.74	148	134
Co_2VGa	0.89	0.20	1.95	1.92	343	352
Co_2MnGa	0.79	2.80	4.29	4.11	698	685
Co_2FeSi	1.30	2.76	5.34	6.00	1134	1100

waves, muffin-tin orbitals, etc. assuming three-dimensional periodicity. For other material classes (like molecular magnets or adatoms on surfaces) other basis sets (localized orbitals) or formalisms (Green function methods) might be better suited. Relativistic calculations (to obtain e.g., spin-orbit coupling effects) or problems dealing with electron-nucleus interaction might profit from an all-electron treatment of the DFT problem, while for obtaining other quantities (spin moments, scalar exchange interactions) a pseudopotential treatment can be sufficient. In most cases, however, the diversity of available DFT implementations will make it easy to find a suitable solution for a specific problem.

2 Methodological Framework

To calculate the electronic structure of an atom, a molecule or a solid, it is necessary to solve the Schrödinger- or Dirac-equation that governs the behavior of the electrons in the system. This behavior is encoded in the wavefunction, Ψ, that is a complex quantity in $3N$-dimensional space if N is the number of electrons. Even for a moderate amount of particles (e.g., 26 electrons in an Fe atom) this many-particle wavefunction is impossible to handle numerically. If spin comes into play, or a time-dependence has to be included, the problem even worsens. Therefore, a straightforward solution is – in most cases – out of reach.

The key idea of density functional theory is to work, instead of the many-body wavefunction, with the density, $n(\mathbf{r})$, as the basic variable. The latter can be obtained by the former by integration over all but one spatial variables:

$$n(\mathbf{r}) = N \int d\mathbf{r}_2 \ldots \int d\mathbf{r}_N \Psi^*(\mathbf{r}, \mathbf{r}_2, \ldots, \mathbf{r}_N)\Psi(\mathbf{r}, \mathbf{r}_2, \ldots, \mathbf{r}_N)\,. \tag{1}$$

Surprisingly, the total energy, E, turns out to be a unique functional of this density and this functional is stationary with respect to variations of $n(\mathbf{r})$. This theorem was worked out by Hohenberg and Kohn (1964), together with the observation that in a non-degenerate ground state the many-body wavefunction Ψ that describes electrons in an external potential, $v(\mathbf{r})$ (caused by e.g., nuclei), is uniquely determined by the particle density distribution $n(\mathbf{r})$ (The charge density is obtained by multiplying n with the electron's charge $-e$. In atomic units this is normalized to unity and in the following e is not written explicitly, unless in the context of some relativistic terms.). The energy functional can be written as

$$E[n(\mathbf{r})] = \int v(\mathbf{r})n(\mathbf{r})d\mathbf{r} + F[n(\mathbf{r})], \tag{2}$$

where the first term on the right side describes the Coulomb interaction of the density with the external potential and the functional F captures the kinetic energy of the electrons and their mutual Coulomb repulsion. Since Hohenberg and Kohn

could show that the density determines $v(\mathbf{r})$ to within a constant, all terms in Eq. (2) can be determined for a given $n(\mathbf{r})$, provided that F is known.

It was the achievement of Kohn and Sham (1965) to find a representation of this functional that allowed to split it into large, known parts and a small, unknown remainder. Their idea was to consider a fictitious system of independent electrons that have the same density, $n(\mathbf{r})$, as the true electron system: Then, the kinetic energy, T_0, and the Coulomb interaction of these electrons can be separated out:

$$F[n(\mathbf{r})] = T_0[n(\mathbf{r})] + \frac{1}{2}\int\int \frac{n(\mathbf{r})n(\mathbf{r}')}{|\mathbf{r}-\mathbf{r}'|} d\mathbf{r}d\mathbf{r}' + E_{\mathrm{xc}}[n(\mathbf{r})] \tag{3}$$

and the remaining so-called exchange-correlation (XC) functional, $E_{\mathrm{xc}}[n(\mathbf{r})]$, is just a small correction to be determined. In reality, the movement of the electrons is correlated due to their Coulomb interaction, not independent, and E_{xc} has to account for this difference. The exchange energy, arising from the fact that the density is derived from a Slater determinant of wavefunctions that will be defined below, is also contained in E_{xc}.

With this decomposition, it is possible to evaluate the (large) term T_0, assuming that the fictitious independent electrons are described by wavefunctions ϕ so that $n(\mathbf{r}) = \sum_{i=1}^{N} |\phi_i(\mathbf{r})|^2$. Hereby, an Aufbau principle is used to occupy the ϕ_i, ensuring that the total wavefunction of the Kohn-Sham system satisfies the Pauli principle. The kinetic energy of the electrons with the mass m is given by $T_0 = -\frac{\hbar^2}{2m}\sum_{i=1}^{N} \phi_i^*(\mathbf{r})\nabla^2\phi_i(\mathbf{r})d\mathbf{r}$. Now, requiring that $E[n(\mathbf{r})]$ is stationary with respect to variations of the ground state density and requiring particle conservation, the resulting Euler-Lagrange equation can be recast in the form of an effective single particle Schrödinger equation, the Kohn-Sham equation:

$$\left[-\frac{\hbar^2}{2m}\nabla^2 + \int \frac{n(\mathbf{r}')}{|\mathbf{r}-\mathbf{r}'|} d\mathbf{r}' + v(\mathbf{r}) + V_{\mathrm{xc}}(\mathbf{r})\right]\phi_i(\mathbf{r}) = \varepsilon_i\phi_i(\mathbf{r})\,. \tag{4}$$

Here, the exchange correlation potential, V_{xc}, is the derived as $\frac{\delta E_{\mathrm{xc}}}{\delta n(\mathbf{r})}$, the ε_i are strictly speaking just Lagrange parameters that follow from the normalization condition; In practice they are often used as 'single particle energies' to describe spectral properties. Equation (4) has to be solved self-consistently since it contains the density (both explicitly and implicitly via the exchange correlation potential) that depends on the single particle wavefunctions. Nevertheless, the numerical effort is rather moderate, comparable to the well-known Hartree equation, i.e., it scales normally with the third power of the system size. In particular, this is much faster than wave-function based methods (Friesner 2005).

2.1 Vector-Spin DFT

Since the magnetic ground-state properties are uniquely determined by the many-body wavefunction that is in turn determined by the density, in principle DFT allows finding out the magnetic order, magnetic moments etc., provided that a method is known to extract these properties from the density. In practice, however, it turns out to be easier to extend DFT in a way that explicitly includes the spin-density, $s(\mathbf{r})$, in the formalism. This has the additional advantage that it gives a handle to calculate not only the magnetic ground state, but also other, metastable, magnetic orders. E.g., it is possible to initialize a DFT calculation of body-centered cubic (bcc) Fe such that ferromagnetic (FM), antiferromagnetic (AFM) or nonmagnetic (NM) solutions and their relative stability are obtained. This turns out to be very useful to access the strength of magnetic interactions in a system.

As an example, in Fig. 1 cuts through the (spin-) density of Fe and Cr are shown in the NM state and in the magnetic ground state that is FM for Fe and AFM for Cr. Clearly, the density alone is not very sensitive to variations of the magnetic state, although for FM Fe a small decrease of hybridization, which is due to the spin-splitting of the states, can be seen in the images. However, in both cases only the spin-density gives a clear picture of the magnetic order.

The spin-dependent version of DFT works with spinor wavefunctions to define the spin density $\mathbf{s}(\mathbf{r})$:

$$\mathbf{s}(\mathbf{r}) = \left\langle \phi(\mathbf{r}) | \underline{\boldsymbol{\sigma}} | \phi(\mathbf{r}) \right\rangle \; ; \quad \phi(\mathbf{r}) = \begin{pmatrix} \phi_\uparrow(\mathbf{r}) \\ \phi_\downarrow(\mathbf{r}) \end{pmatrix} . \tag{5}$$

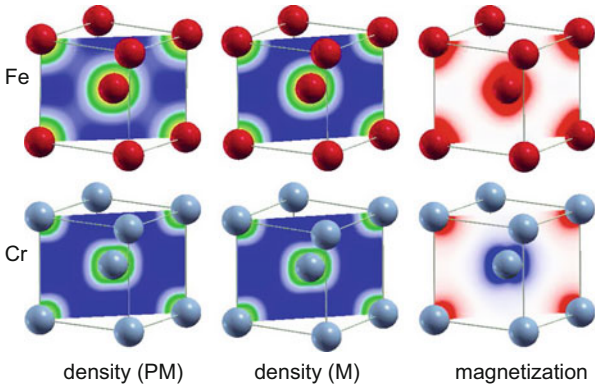

Fig. 1 (110) cuts through the density and magnetization of bcc Fe and bcc Cr. The left and middle columns show the densities in the nonmagnetic (NM) and magnetic (M) state, respectively, where blue color indicated low density and green/yellow high density. In the right column the magnetization is plotted, where red (blue) color encodes positive (negative) values. The plots were obtained using the FLEUR-code for the DFT calculations (Kurz et al. 2004) and XCrysDen for plotting (Kokalj 2003)

(The magnetization density is obtained by multiplying $-\mathbf{s}$ with the Bohr magneton, $\mu_\mathrm{B} = \frac{e\hbar}{2mc}$.) Here, the Pauli matrices (underlined symbols denote 2×2 matrices) are given as:

$$\underline{\sigma_x} = \begin{pmatrix} 0 & 1 \\ 1 & 0 \end{pmatrix}, \quad \underline{\sigma_y} = \begin{pmatrix} 0 & -i \\ i & 0 \end{pmatrix}, \quad \underline{\sigma_z} = \begin{pmatrix} 1 & 0 \\ 0 & -1 \end{pmatrix}. \tag{6}$$

With this, a density matrix can be introduced that is composed of a scalar and a vectorial part, corresponding to the particle and spin density:

$$\underline{n}(\mathbf{r}) = \frac{1}{2}\left(n(\mathbf{r})\underline{\mathrm{I}} + \underline{\boldsymbol{\sigma}} \cdot \mathbf{s}(\mathbf{r})\right) = \frac{1}{2}\begin{pmatrix} n(\mathbf{r}) + s_z(\mathbf{r}) & s_x(\mathbf{r}) - is_y(\mathbf{r}) \\ s_x(\mathbf{r}) + is_y(\mathbf{r}) & n(\mathbf{r}) - s_z(\mathbf{r}) \end{pmatrix}, \tag{7}$$

where $\underline{\mathrm{I}}$ denotes a 2×2 unit matrix. It is easy to see that the components of the density matrix are given by $n_{\alpha\beta}(\mathbf{r}) = \phi^*_\alpha(\mathbf{r})\phi_\beta(\mathbf{r})$ where α, β are spin labels. Analogously, a potential matrix, denoted as $\underline{v}(\mathbf{r})$, can be written in terms of a scalar potential, v, and magnetic field, $\mathbf{B}(\mathbf{r})$:

$$\underline{v}(\mathbf{r}) = v(\mathbf{r})\underline{\mathrm{I}} - \mu_B \underline{\boldsymbol{\sigma}} \cdot \mathbf{B}(\mathbf{r}). \tag{8}$$

In terms of these quantities, von Barth and Hedin (1972) extended DFT to spin-polarized systems. They derived an analog to Eq. (4) in the form:

$$\left[\left(-\frac{\hbar^2}{2m}\nabla^2 + \int \frac{n(\mathbf{r}')}{|\mathbf{r} - \mathbf{r}'|} d\mathbf{r}'\right)\underline{\mathrm{I}} + \underline{v}(\mathbf{r}) + \underline{V}_\mathrm{xc}(\mathbf{r})\right]\begin{pmatrix} \phi_i^\uparrow(\mathbf{r}) \\ \phi_i^\downarrow(\mathbf{r}) \end{pmatrix} = \varepsilon_i \begin{pmatrix} \phi_i^\uparrow(\mathbf{r}) \\ \phi_i^\downarrow(\mathbf{r}) \end{pmatrix}, \tag{9}$$

where $\underline{V}_\mathrm{xc}$ is now defined as the functional derivative of the exchange-correlation energy with respect to the density matrix. If $\underline{v}(\mathbf{r})$ and $\underline{V}_\mathrm{xc}(\mathbf{r})$ are diagonal matrices, Eq. (9) clearly decomposes into two equations of type (4) for spin-up and spin-down wavefunctions.

Naturally the quality of the results obtained with Eq. (9) depends heavily on the approximation for $\underline{V}_\mathrm{xc}$. In the local density approximation (LDA) or, for the spin-polarized case, the local spin density approximation (LSDA), the exchange correlation energy is assumed to be of the form

$$E_\mathrm{xc}^{LSDA} = \int n(\mathbf{r})\varepsilon_\mathrm{xc}\left[n_\uparrow(\mathbf{r}), n_\downarrow(\mathbf{r})\right] d\mathbf{r}, \tag{10}$$

where ε_xc is the exchange correlation energy density of the homogeneous, spin-polarized electron gas. Already before the formulation of DFT several approximations have been known for the exchange energy of the homogeneous electron gas, e.g., from the Thomas-Fermi-Dirac theory (Dirac 1930) or derived from Hartree-Fock theory (Slater 1951). In all these cases it was observed that $\varepsilon_\mathrm{x} \propto [n(\mathbf{r})]^{1/3}$

and, surprisingly, the first LDA functionals based on this approximations performed rather well.

Although modern exchange correlation functionals are more sophisticated, many properties of spin-polarized DFT calculations can be studied already in the simple LSDA form. Suppose, there is a collinear magnet with the orientation of the magnetization in z-direction (actually, the Hamiltonian in Eq. (9) is invariant under spin-rotations). Then, the density matrix is diagonal and $\underline{V}_{\rm xc}$ has only two terms: $V_{\rm xc}^{\uparrow\uparrow} = \frac{\delta E_{\rm xc}}{\delta n_{\uparrow\uparrow}} \propto \left[n_{\uparrow\uparrow}(\mathbf{r})\right]^{1/3}$ and $V_{\rm xc}^{\downarrow\downarrow} = \frac{\delta E_{\rm xc}}{\delta n_{\downarrow\downarrow}} \propto \left[n_{\downarrow\downarrow}(\mathbf{r})\right]^{1/3}$. This means that Eq. (9) consists of two equations, one for $\phi_\uparrow$ and one for $\phi_\downarrow$ that are identical if $n_{\uparrow\uparrow} = n_{\downarrow\downarrow}$, i.e., if the charge density is not spin-polarized. If a self-consistent calculation starts from a non-magnetic density it remains in this state, even if a spin-polarized solution gives a lower total energy. This shows that the spin-polarized version of DFT can lead to metastable solutions and it is necessary to break the symmetry of the spin-channels to arrive at a magnetic ground state.

Some DFT results for ferromagnetic elements are shown in Table 2, where both the LSDA moments are listed and values obtained within the generalized gradient approximation (GGA) to the exchange-correlation potential. Although the more sophisticated GGA functionals usually lead to better predictions of the atomic structure or lattice constants, the magnetic properties are in most cases not improved (Singh and Ashkenazi 1992). Systematic studies of magnetic properties with modern XC potentials are rather scarce, but it seems that at least in some cases care has to be taken (Koller et al. 2011). This is not surprising, since most efforts are devoted to improving the description of structural parameters or binding energies in these functionals and often the performance with respect to magnetic properties is not tested. There are developments of new functionals that can, in principle, improve also the description of non-collinear magnetism (Eich and Gross 2013), however with considerably increased numerical efforts.

Table 2 Magnetic moments (in $\mu_{\rm B}$ per atom) of ferromagnetic elements in the bulk. The experimentally determined total magnetization, $M_{\rm tot.}$, consists of spin- and orbital moment contributions. The LSDA results for Fe, Co and Ni are taken from Moruzzi et al. (1978), the GGA values of the magnetic moments from Shallcross and coworkers (2005), the experimental values are quoted from Trygg et al. (1995). The calculated Gd moments are from Kurz et al. (2002), the experimental one is taken from White and coworkers (1975)

Property	Source	Fe (bcc)	Co	Ni (fcc)	Gd (hcp)
$M_{\rm spin}$	LSDA	2.15	1.56 (fcc)	0.59	7.63
$M_{\rm spin}$	GGA	2.22	1.62 (fcc)	0.62	7.65
$M_{\rm spin}$	Experiment	2.13	1.52 (hcp)	0.57	
$M_{\rm tot.}$	Experiment	2.21	1.66 (hcp)	0.62	7.63

2.2 Spin-Orbit Coupling

It was already mentioned in the last section that the Hamiltonian in Eq. (9) has several shortcomings: Since it is derived from the Schrödinger equation, there is no spin-dependent term in this Hamiltonian; Spin enters just through the wavefunction and the Pauli-principle that is encoded in the exchange part of the XC potential. This is enough to find out that Fe is ferromagnetic and has a (spin-) moment of 2.2 μ_B, but this moment has no preferential direction. The concept of easy and hard magnetic directions enters only if further, spin-dependent terms are added to the Hamiltonian. Thinking in terms of a general interaction between two classical spins, $\mathbf{S}$, of the form $\mathbf{S}_\nu \underline{J}_{\nu\nu'} \mathbf{S}_{\nu'}$, where $\underline{J}$ is a 3×3 matrix, only the trace of $\underline{J}$ can be accessed by Eq. (9). This gives rise to Heisenberg-type interactions of the form $J_{\nu\nu'} \mathbf{S}_\nu \cdot \mathbf{S}_{\nu'}$ that are in many cases responsible for the magnetic order and, for $\nu = \nu'$, it describes the intra-atomic exchange interaction that is responsible for the formation of the magnetic moment.

To go beyond this description, it is necessary to start from the Dirac-equation or, if one wants to keep two-component wavefunctions, the Pauli-equation that can be derived from the Dirac-equation keeping terms up to second order in c, the velocity of light. (We consider here the single-particle equations, adopting the view that the Kohn-Sham equations are also in a single-particle form that can be extended by relativistic terms.) The Hamiltonian of the Pauli-equation can be written as (Bethe and Salpeter 1977):

$$H_{\text{Pauli}} = H_{\text{NR}} + H_{\text{SR}} + \frac{\hbar}{(2mc)^2} \underline{\boldsymbol{\sigma}} \cdot (\boldsymbol{\nabla} V(\mathbf{r}) \times \mathbf{p}) - \frac{e\hbar}{2mc} \underline{\boldsymbol{\sigma}} \cdot \mathbf{B}(\mathbf{r}) \,. \tag{11}$$

Here, H_{NR} is the usual Schrödinger-type Hamiltonian (with the momentum operator $\mathbf{p}(\mathbf{r})$ extended by the vector potential $\frac{e}{c}\mathbf{A}(\mathbf{r})$) and H_{SR} contains scalar-relativistic terms that do not contain spin-operators:

$$H_{\text{SR}} = -\frac{1}{2mc^2} \left(E + eV(\mathbf{r})\right)^2 + \frac{\hbar^2}{8m^2c^2} \nabla^2 V(\mathbf{r}) \,. \tag{12}$$

These are the mass-velocity correction containing the non-relativistic energy E and the Darwin term, relevant mostly for s electrons. The last two terms in Eq. 11 represent the spin-orbit interaction and the interaction of the spin with an external magnetic field. This last term was already included ad hoc in the potential matrix $\underline{v}(\mathbf{r})$. It may seem odd that in DFT calculations the magnetic field is normally considered via this B-field, while the mentioned vector potential contribution is neglected. Indeed, the latter is responsible for diamagnetic effects and has been discussed in the context of calculating NMR shielding tensors (Pickard and Mauri 2001), but requires a rather special treatment that goes beyond this introduction.

The physical interpretation of the spin-orbit coupling (SOC) term in Eq. (11) is most easily seen in an atom, where the gradient of the central potential can be written $\boldsymbol{\nabla} V(\mathbf{r}) = \frac{\partial V(r)}{\partial r} \frac{\mathbf{r}}{r}$. Then,

$$\frac{\hbar}{(2mc)^2}\underline{\boldsymbol{\sigma}} \cdot (\boldsymbol{\nabla} V(\mathbf{r}) \times \mathbf{p}) = \frac{\hbar}{(2mc)^2}\frac{1}{r}\frac{\partial V(r)}{\partial r}\underline{\boldsymbol{\sigma}} \cdot (\mathbf{r} \times \mathbf{p}) = \xi \underline{\boldsymbol{\sigma}} \cdot \mathbf{L}, \tag{13}$$

where ξ is called the SOC constant and $\mathbf{L} = \mathbf{r} \times \mathbf{p}$ is the (angular) orbital momentum operator. In this form, the SOC term resembles a coupling between spin- and orbital momentum, although one has to keep in mind that it is rather the (orbital) motion of the electron in a potential gradient (i.e., an electric field that is Lorentz-transformed into a magnetic field) that couples to the spin. This also applies to a linear motion of an electron, where the SOC term manifests in the so-called Rashba-effect (Bychkov and Rashba 1984).

Due to this coupling between the potential landscape (as, e.g., formed by the atomic lattice in a solid) and the electron spin, the orientation of the magnetization in the solid is no longer arbitrary but certain directions are preferred. This is one source of magnetic anisotropy, the so-called magnetocrystalline anisotropy, that determines the 'easy axis' of magnetization. (Other sources, like the dipole-dipole interaction are not included in the single particle equation (11) and have to be added, e.g., from a classical calculation of the dipole sum.)

The effect of spin-orbit interaction in a magnetic system can be seen as a certain symmetry breaking that leads not only to a magnetic anisotropy, but also other effects like magnetostriction. This can be seen most clearly from a consideration of the band structure in two directions that are equivalent without SOC, but get non-equivalent when SOC is taken into account. As an example Fig. 2 shows the band structure of bulk bcc Fe along a high-symmetry direction in reciprocal space ($\Gamma - H$). In this direction, without SOC, several band crossings can be detected, e.g., between $d_{x^2-y^2}$ states and d_{xy} states of same and different spin. The SOC

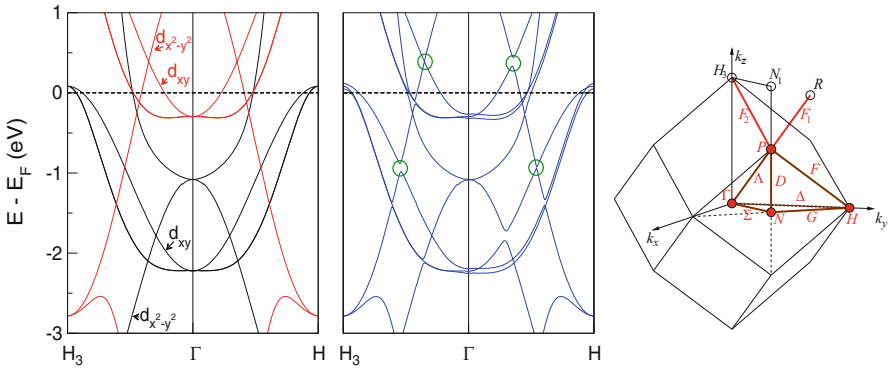

Fig. 2 Band structure of bcc Fe without (left) and with (middle) SOC effects. The Brillouin zone is shown on the right. (From the Bilbao Crystallographic Server, http://www.cryst.ehu.es). Left: Majority and minority spin states are shown in black and red, respectively. The character of the orbitals forming the bands along $\mathsf{H}_3 - \Gamma$ is indicated. With SOC the spin-character of the states is mixed and some band degeneracies are lifted. Crossings discussed in the text are marked with green circles. The magnetization is assumed to point in y direction

term, Eq. (13), allows now hybridization between these states of the same spin to form an orbital moment in the direction of magnetization ($\Gamma - H$ corresponding to y) and these states of opposite spin in $\Gamma - H_3$ direction. Thus, gaps form at different positions in the formerly equivalent directions, which leads to a symmetry reduction from cubic to tetragonal in this case. These gap openings were recently also seen experimentally (Młyńczak et al. 2016).

Moreover, the spin-orbit terms gives rise to a finite orbital momentum that can be easily obtained in the vicinity of an atom ν as

$$\mathbf{M}_\nu^{\mathrm{orb}} = -\mu_\mathrm{B} \sum_i \langle \phi_i | \mathbf{L} | \phi_i \rangle_\nu \tag{14}$$

where the integration is performed in a sphere around the atom. To obtain the orbital moment in an infinite periodic solid a more involved theory is necessary (Thonhauser et al. 2005). It should be noted that the orbital moments obtained by LSDA (and also GGA) calculations are typically too small, e.g., for Fe and Co values of 0.05 and 0.08 μ_B have been obtained (Beiden et al. 1998). Compared to experimental values (i.e., the difference between total and spin-momentum in Table 2) these values are reduced by almost 50%.

In absence of spin-flip terms (i.e., when the majority and minority band are well separated by the exchange interaction), SOC changes the total energy of a system in second-order perturbation theory as (van der Laan 1998):

$$\delta E = \sum_{i,j} \frac{\langle \phi_i | H_\mathrm{so} | \phi_j \rangle \langle \phi_j | H_\mathrm{so} | \phi_i \rangle}{\varepsilon_i - \varepsilon_j} f(\varepsilon_i) \left[1 - f(\varepsilon_j)\right] \approx -\frac{1}{4} \xi \hat{\mathbf{S}} \cdot \left[\left\langle \mathbf{L}^\downarrow \right\rangle - \left\langle \mathbf{L}^\uparrow \right\rangle \right] \tag{15}$$

where H_so is the SOC Hamiltonian, f is the Fermi function giving the occupation of the state, $\hat{\mathbf{S}}$ is the direction of the spin moment, and $\mathbf{L}^{\downarrow(\uparrow)}$ is the orbital moment of the spin-down (up) bands. If the spin-up band is completely filled, we see that energy change, δE, is proportional to the size of the orbital moment. The magnetocrystalline anisotropy energy (MAE), i.e., the difference of δE for two different magnetization directions, will be proportional to the difference in the orbital moments as first derived by Bruno (1989).

When calculating the MAE from DFT one has to keep in mind that the resulting energy differences are often very small, for cubic metals like Fe or Ni even in the μeV per unit cell range (see Table 3). Therefore, the numerical parameters, in particular those determining the sampling of reciprocal space, have to be extremely well converged (Trygg et al. 1995). To make the numerical effort tractable, often these calculations are not performed self-consistently, but SOC is added on top of a non- or scalar-relativistic calculation using the so-called force theorem (Weinert et al. 1985). Although the experimental values of the MAE for the cubic elements listed in Table 3 are hard to reproduce quantitatively, the easy axis is correctly reproduced in LSDA (Halilov et al. 1998).

Table 3 Magnetic anisotropy energy (in μeV per atom) of the ferromagnetic elements obtained by DFT calculations with spin-orbit (SO) coupling included as obtained by Trygg et al. (1995) [1] and Halilov et al. (1998) [2]. In addition, the results including the orbital polarization correction (OP) are cited from [1]. The experimental data (exp.) are quoted from both references. For the fcc structures the anisotropy between [001] and [111] direction is given and positive values indicate that the latter magnetization direction is preferred. The values for Co (hcp) show the energy difference between the [0001] and [10$\bar{1}$0] direction

Element	SO[1]	OP[1]	SO[2]	exp.
Fe (bcc)	–0.5	–1.8	–2.6	–1.4
Co (hcp)	–29	–110		–65
Co (fcc)	0.5	2.2	2.4	1.3–1.8
Ni (fcc)	–0.5	–0.5	1.0	2.7

Table 4 Magnetic anisotropy energy (in meV per formula unit) of the $L1_0$ phases of FePt and CoPt obtained in LSDA with spin-orbit (SO) coupling and orbital polarization (OP) by Ravindran et al. (2001) [1], Shick and Mryasov (2003) [2] and Kota and Sakuma (2014) [3], where perturbation theory (PT) and force theorem (FT) were used. Positive numbers indicate that the [001] direction is preferred (relative to [100]). The experimental data (exp.) are quoted from Ravindran et al. (2001)

Element	SO[1]	OP[1]	SO[2]	PT[3]	FT[3]	Exp.
FePt	2.73	2.89	2.68	2.41	1.90	0.88
CoPt	1.05	1.64	1.03	0.77	0.68	1.0–1.67
FePd	0.15	0.34		0.33	0.29	0.48–0.63

As suggested by Eq. (15), the underestimation of the orbital moments in LSDA also leads to MAEs that are systematically too small. Techniques like the orbital polarization correction (OP) were introduced that increase both quantities leading to better agreement with experimental values (Trygg et al. 1995). Another way to improve results is to tale into account strong correlation effects via the Hubbard U approximation (LSDA+U), as shown by Yang et al. (2001) or, for binary alloys by Shick and Mryasov (2003). For uniaxial systems, where the energies go up to the meV scale, the agreement is generally better as can be seen from Table 4.

Although in the examples listed above only the energies of two magnetization directions were compared, the MAE describes more generally the dependence of the energy on the spin orientation. In terms of the general two-spin interaction, $\underline{J}_{\nu\nu'}$, the magnetic anisotropy can be expressed as the traceless symmetric on-site part ($\nu = \nu'$) denoted as $\underline{K}_{\nu}$. It is a matrix with (at most) six coefficients that can be obtained by independent calculations.

One should keep in mind that a DFT calculation with SOC also gives rise to interactions described by the symmetric part of the $\underline{J}$ matrix (so-called pseudodipolar interactions) and the antisymmetric part of the $\underline{J}$ [Dzyaloshinskii-Moriya interaction (Dzialoshinskii 1957)] where the strength of the latter is first order in SOC, while the former arises in second order (Moriya 1960). Although small, these interactions can be extracted from DFT calculations as will be outlined below.

3 Ground State Calculations

3.1 Magnetic Order

It was shown that spin-polarized versions of DFT allow calculating also metastable magnetic (or non-magnetic) configurations and the result depends on the initial configuration. This makes determining the magnetic ground state of a specific system by DFT a rather challenging problem. Different strategies can be applied: like in molecular-dynamics calculations, (ab initio) spin-dynamics allows exploring the magnetic degrees of freedom and finding the global energy minimum that corresponds to the ground state configuration. A different possibility is to determine the magnetic interactions between the atoms by DFT calculations which are then mapped onto a model (in the simplest case a classical Heisenberg model) that is solved analytically or numerically. In both cases a discretization of the (vector) magnetization density in terms of magnetic moments is introduced. Assume that at the positions of the magnetic atoms the intra-atomic exchange interaction is large and there are robust magnetic moments that can be assigned to each lattice site, e.g., within some sphere centered at the nucleus, ν (at a position $\mathbf{R}_\nu$). Then the magnetization density, $\mathbf{m}(\mathbf{r})$, can be approximated as

$$\mathbf{m}(\mathbf{r}) = M_\nu \hat{\mathbf{e}}_\nu, \tag{16}$$

where M_ν is the magnetization and $\hat{\mathbf{e}}_\nu$ is the magnetization direction at that site. A magnetic state is in this case characterized by a set of directions, $\{\hat{\mathbf{e}}_\nu\}$, of all the atoms in the magnetic unit cell. Of course there are the well-known ferromagnetic (FM) and antiferromagnetic (AFM) states, but already for the latter several possible unit cells come in mind. E.g., in an face-centered cubic (fcc) material, an AFM order can occur for ferromagnetically ordered planes in (001), (111), or (110) directions (type I, II or III AFM order, respectively) to name just the few possibilities that can be realized by a Heisenberg model with nearest-neighbor (nn) and next-nearest-neighbor (nnn) interactions.

On a simple level, one can "relax" the directions of the magnetization at the atoms like a relaxation of the atomic structure (e.g., at a surface) is done. In the DFT self-consistency cycle the output magnetizations $\{\hat{\mathbf{e}}_\nu^{\text{out}}\}$ in general deviate from the input values $\{\hat{\mathbf{e}}_\nu^{\text{in}}\}$. The magnetization directions change to minimize the total energy (cf. Fig. 3). The final magnetic state, that is reached, in general depends on the starting point of the calculation and a more elaborate technique is needed to avoid being trapped in some local minimum of $E[\{\hat{\mathbf{e}}_\nu\}]$.

To this end one can develop an equation of motion for the magnetization of an atom. To keep things simple it is again assumed that the magnetization stays collinear within the vicinity of the atom. Starting from the Hamiltonian of Eq. (9) and assuming that the external potential matrix, $\underline{v}(\mathbf{r})$, has been chosen to be diagonal and the exchange-correlation potential is separated into diagonal and off-diagonal

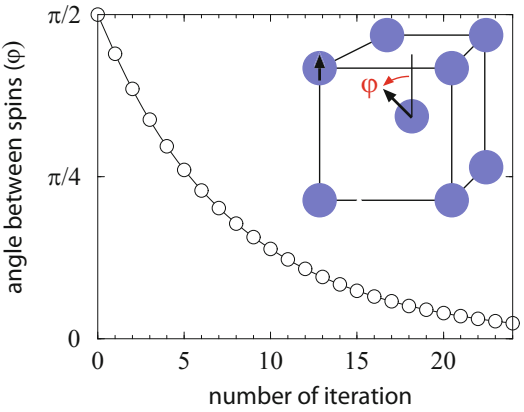

Fig. 3 Relaxation of the spin direction of a Fe atom in bulk bcc Fe calculated in a simple cubic unit cell. The evolution of the angle φ between the magnetic moments of two Fe atoms is shown as a function of the number of the self-consistency steps of the DFT calculation. Starting from a 90° canting of the spins, the FM ground state is reached after approx. 30 iterations. It is important to avoid high-symmetry states (e.g., AFM) as starting points. (Adapted with permission from Kurz et al. 2004. Copyrighted by the American Physical Society)

parts, following Antropov et al. (1995, 1996) it is possible to set up a time-dependent analog of Eq. (9):

$$i\frac{d\Phi}{dt} = \left[H_d - \underline{\boldsymbol{\sigma}} \cdot \mathbf{B}(\mathbf{r}, t)\right]\Phi \quad \text{where} \quad \Phi = \begin{pmatrix} \phi_\uparrow(\mathbf{r}, t) \\ \phi_\downarrow(\mathbf{r}, t) \end{pmatrix}, \tag{17}$$

and H_d is the Hamiltonian that contains now only diagonal parts.

Separating the evolution of the magnetization into fast (value of the magnetization) and slow (direction of the magnetization) degrees of freedom the fast part are described quantum-mechanically, while the latter can be treated on a semiclassical level. At a given time, t, the time-independent version of Eq. (17) can be solved for a given magnetization characterized by $\{\hat{\mathbf{e}}_v\}$. An equation of motion for the magnetization $\mathbf{m}(\mathbf{r}, t)$ can be obtained by multiplying Eq. (17) from the left with $-\mu_B \Phi^* \underline{\boldsymbol{\sigma}}$ and adding the complex conjugate equation. Comparing to the time derivative of the magnetization (cf. Eq. (5)), the equation of motion reads

$$\frac{d\mathbf{m}(\mathbf{r}, t)}{dt} = 2\mathbf{m} \times \mathbf{B} + \frac{i}{2}\nabla(\Phi^* \underline{\boldsymbol{\sigma}} \cdot \nabla\Phi - c.c.). \tag{18}$$

The second term on the right side is complicated and describes longitudinal changes of the magnetization, which will not be considered on this level. Omitting this term, Eq. (18) describes the precession of the magnetization direction at an atom under the influence of the magnetic field generated by the atom itself and other atoms of the crystal.

Equation (18) can be simplified using Eq. (16) and one can write for the evolution of the magnetization direction in atom ν

$$\frac{d\hat{\mathbf{e}}_\nu}{dt} = -\frac{2}{\mu_\mathrm{B}}\hat{\mathbf{e}}_\nu \times \mathbf{I}_\nu, \tag{19}$$

where $\mathbf{I}_\nu = \mu_\mathrm{B}\mathbf{B}$. If the effect of other fields acting on a magnetization direction has to be taken into account explicitly, they can be included in Eq. (19). E.g., for contributions stemming from the spin-orbit interaction (magnetic anisotropy) or dipole-dipole interaction, these fields can be added in the form $\mathbf{I} = \mathbf{I}_\nu + \mathbf{I}_\mathrm{SO} + \mathbf{I}_\mathrm{d-d}$. More general expressions of Eq. (19), suitable for spin-dynamics with finite temperatures included, can be found in the paper of Antropov et al. (1996). It should be noted that these equations are the starting point to describe many properties beyond the ground state on an ab initio basis e.g., shown by Skubic et al. (2008).

3.2 Magnetic Interactions

Although spin-dynamic simulations are a good way to explore magnetic ground states, they are computationally rather expensive and require additional analysis to get insight into the interactions leading to a specific magnetic order. For an interpretation of the results the system is usually mapped to a classical model spin Hamiltonian, e.g.,

$$H_\mathrm{mod} = -\sum_{\langle\nu\nu'\rangle} J_{\nu\nu'}\mathbf{M}_\nu \cdot \mathbf{M}_{\nu'} + \sum_\nu \mathbf{M}_\nu \underline{K}_\nu \mathbf{M}_\nu + \sum_\nu \mathbf{B}\cdot\mathbf{M}_\nu, \tag{20}$$

where the first term on the right side captures the Heisenberg-like (scalar, two-spin) interactions and the sum runs over all pairs of atoms $\langle\nu, \nu'\rangle$, the second term is the magnetic anisotropy and the last term represents the interaction of the spins with an external $\mathbf{B}$ field (if needed). As mentioned above, the magnetic moments $\mathbf{M}_\nu$ are directly available from the DFT results and the anisotropy $\underline{K}_\nu$ can be obtained from relativistic total energy calculations.

To extract the $J_{\nu\nu'}$ coefficients in Eq. (20), it is in principle possible to compare the total energies of ferromagnetic and different antiferromagnetic states from non-relativistic DFT calculations and fit these differences to a classical spin Hamiltonian. As example in Fig. 4 the case of a square lattice is shown, as e.g., realized by an Fe monolayer on a (001) oriented bcc substrate. Ferriani et al. (2007) studied this system for Ta and W as substrate and found a transition from a FM ground state for Ta to a $c(2\times 2)$ AFM state for Fe/W(001). In a nearest-neighbor (nn) Heisenberg model this transition corresponds to a sign change of the nn coupling constant J_1. Including also next-nearest-neighbor (nnn) interactions, this model also allows (for negative J_2) for another ground state, a row-wise AFM state with a $p(2\times 1)$ unit cell as shown in Fig. 4. By calculating these three magnetic states for alloyed substrates, $\mathrm{Ta}_x\mathrm{W}_{1-x}$, one can see that from $x = 1$ to $x = 0$ J_1 changes from about $+20$

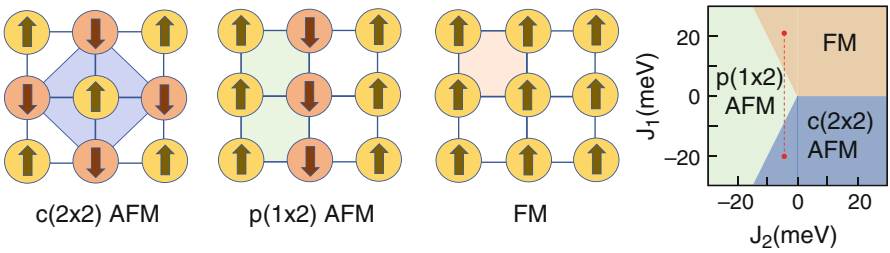

Fig. 4 Two antiferromagnetic (AFM) and the ferromagnetic (FM) structure on a square lattice. The magnetic unit cells are indicated by the shaded areas. The phase diagram for the classical Heisenberg model with nearest-neighbor (nn) and next-nearest-neighbor (nnn) interaction is shown on the right. The red dashed line indicates a phase transition as discussed in the text. (Adapted with permission from Ferriani et al. 2007. Copyrighted by the American Physical Society)

to -20 meV while J_2 remains rather constant at -5 meV. In the phase diagram in Fig. 4 this corresponds to a change along the red dashed line and one can see that for $x = 0.5$ a $p(2\times1)$ AFM structure can be expected as magnetic ground state (Ferriani et al. 2007) (Fig. 5).

Of course, more magnetic structures can be added to the analysis and further interactions, J_i for $i > 2$, can be extracted. A systematic way to obtain these J's is given by the calculation of so-called spiral spin-density waves (SSDWs), general solutions of the classical Heisenberg model. The magnetic moments in a spiral with propagation vector $\mathbf{q}$ are given as:

$$\mathbf{M}_\nu = M\left(\hat{\mathbf{e}}_x \cos(\mathbf{q}\cdot\mathbf{R}_\nu) + \hat{\mathbf{e}}_y \sin(\mathbf{q}\cdot\mathbf{R}_\nu)\right), \tag{21}$$

where the unit vectors $\hat{\mathbf{e}}_x$ and $\hat{\mathbf{e}}_y$ just have to be perpendicular to each other, otherwise their directions are (in absence of SOC) arbitrary. For simplicity it is assumed that the size of the magnetic moment, M, is not site dependent. The wave-length of the spin-spiral is given by $\lambda = \frac{2\pi}{q}$ and it seems that huge super-cells are necessary to capture these SSDWs. But using the generalized Bloch theorem (Herring 1966; Sandratskii 1991) these magnetic structures can be conveniently calculated in the chemical unit cell as long as no spin-orbit coupling is considered. In this way the total energy $E(\mathbf{q})$ can be calculated on a grid of $\mathbf{q}$ vectors and, assuming that M remains constant, directly related to $J(\mathbf{q})$ which is the Fourier transform of the Heisenberg interaction constants in real space. By Fourier transformation the constants $J_{\nu\nu'}$ can thus be recovered. This procedure can be generalized to systems with different atomic species in the unit cell, where intra-sublattice J's and inter-sublattice J's have to be considered (Ležaić et al. 2013).

Spin-spiral structures, as given by Eq. (21), also occur as ground states in many magnetic systems. A well-investigated system is bcc Eu, a member of the lanthanides, where the spins are rotated between neighboring (001) planes by 47° (Turek et al. 2003b). DFT calculations of SSDWs with $\mathbf{q}$ along the $(1, 0, 0)$ direction indeed show a minimum of $E(\mathbf{q})$ at the experimentally observed position.

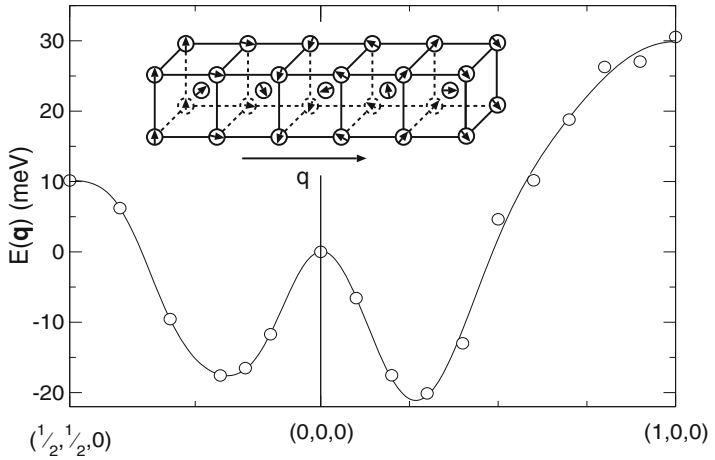

Fig. 5 Total energy of bcc-Eu as a function of the spin-spiral $\mathbf{q}$-vector (in units of $\frac{2\pi}{a}$ where a is the lattice constant) in (110) and (100) direction calculated in the LDA+U method. The symbols represent calculated values, the lines are a fit of $E(q) = \sum_{n=0}^{5} c_n \cos(n\pi q)$. The energy minimum at $\mathbf{q} = (1.63, 0, 0)/a$ (also visualized in the inset) corresponds quite well to the experimental ground state (Turek et al. 2003b)

Also along the (1, 1, 0) direction a local minimum is found and experiments indeed report that under an external magnetic field such state can be realized (Millhouse and McEwen 1973). It should be further mentioned that in these calculations the so-called LDA+U method (Anisimov et al. 1997) was used to capture the correlated nature of the $4f$ electrons in Eu.

As mentioned above, SSDWs are the general solutions of the classical Heisenberg model (Yosida 1996). Therefore, if a system described by this model, a procedure to find the magnetic ground state was presented. However, for a system with spins larger than 1/2, higher order interactions are allowed that involve more than two spins, e.g., the biquadratic interaction $B_{\nu\nu'}(\mathbf{S}_\nu \cdot \mathbf{S}_{\nu'})^2$ or other four-spin interactions. These terms can couple two or more spin-spirals and possibly lead to solutions with lower energy than all SSDWs. E.g., the $p(2 \times 1)$ structure in Fig. 6 can be regarded as spin spiral with $\mathbf{q}_1 = \left(0, \frac{1}{2}\right)$ and a 90° rotated SSDW with $\mathbf{q}_2 = \left(\frac{1}{2}, 0\right)$ is degenerate with this structure. A linear combination $\frac{1}{2}(\mathbf{q}_1 + \mathbf{q}_2)$, where the spins of neighboring atoms are 90° rotated to each other (see Fig. 6), is energetically degenerate to the constituting spin spirals in the classical Heisenberg model, but a Hamiltonian that includes the biquadratic interaction can differentiate between the former double-$\mathbf{q}$ and the latter single-$\mathbf{q}$ structures. In a DFT calculation it is found that indeed the double-$\mathbf{q}$ structure has lower total energy (Ferriani et al.

2007). This is a sign for the importance of higher-order interactions that is not unexpected in a system with large spin moment.

All SSDWs and the AFM structures shown in Fig. 4 [that are actually spin spirals with $\mathbf{q}_{c(2\times2)} = \left(\frac{1}{2}, \frac{1}{2}\right)$, $\mathbf{q}_{p(1\times2)} = \left(\frac{1}{2}, 0\right)$ and $\mathbf{q}_{\mathrm{FM}} = (0, 0)$] are special in the sense that in these structures there is no torque on the magnetic moments due to symmetry. I.e., in the DFT self-consistency cycle the spin direction does not change in the sense described in Sect. 3.1. This is different for the spin-structures that connect the states shown in Fig. 6. To calculate the total energy of such spin structures correctly, constrained DFT calculations (Dederichs et al. 1984) have to be performed, i.e., a transversal $\mathbf{B}_\perp$ field has to be applied that keeps the local moment in a prescribed direction (Kurz et al. 2004). This constrained DFT scheme can also be used to study longitudinal fluctuations of the magnetic moments, $E(|\mathbf{M}|)$. These so-called fixed spin-moment calculations can be very useful to explore magnetic phases, in particular when multiple solutions (high-spin and low-spin phases) are present (Moruzzi et al. 1986).

It was mentioned above that SSDW calculations using the generalized Bloch theorem can only be performed in the absence of SOC. Nevertheless, it is possible to include SOC in first order perturbation theory to the spin-spiral calculations (Heide et al. 2009). In this way, it is possible to access the Dzyaloshinskii-Moriya interaction (DMI) mentioned at the end of Sect. 2.2 in a rather systematic way. This relativistic interaction can then be added to the model Hamiltonian (20) to describe large-scale spin structures. For example the DMI can stabilize a SSDW with unique rotational sense (Bode et al. 2007) or it leads to chiral magnetic skyrmions in complex superlattices with several nanometers of diameter (Dupé et al. 2016). It can also be used as input for micromagnetic simulations of even larger systems (see Schweflinghaus et al. (2016) for an relation of atomistic and micromagnetic parameters).

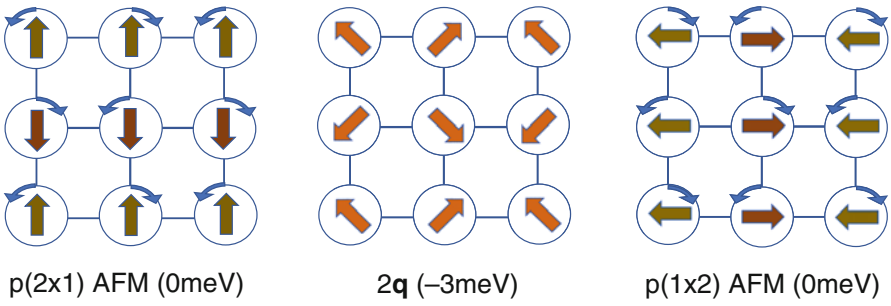

Fig. 6 The 2**q** structure shown in the middle is a superposition of the $p(2 \times 1)$ and $p(1 \times 2)$ structure. Alternatively, it can be constructed by rotation of the spins in the collinear structures by 45° as indicated by the blue arrows. For Fe on a Ta/W-alloy substrate, the 2**q** structure is 3 meV lower in energy than the two shown antiferromagnetic structures (Ferriani et al. 2007)

4 Beyond the Ground State

Although a more detailed account of spin excitations and finite temperature magnetism will follow in the next chapters, this section is intended to show the link between non-collinear DFT calculations, as described above, and the modeling of properties beyond the magnetic ground state. Moreover, the application range and limitations of some simple models are indicated.

4.1 Magnetic Fluctuations

Up to now, flat spin-spirals as defined in Eq. (21) were discussed, i.e., the spins were assumed to be rotating in the plane defined by $\hat{\mathbf{e}}_x$ and $\hat{\mathbf{e}}_y$. These SSDWs can be generalized to conical spin-spirals as

$$\mathbf{M}_\nu = M\left(\hat{\mathbf{e}}_x \cos(\mathbf{q}\cdot\mathbf{R}_\nu)\sin(\vartheta) + \hat{\mathbf{e}}_y \sin(\mathbf{q}\cdot\mathbf{R}_\nu)\sin(\vartheta) + \hat{\mathbf{e}}_z\cos(\vartheta)\right), \tag{22}$$

where 2ϑ defines the opening angle of the cone. Magnetic structures described by Eq. (22) occur as magnetic ground states, e.g., in $LaMn_2Ge_2$ (Di Napoli et al. 2004), or in strong magnetic fields as described by the Hamiltonian (20).

Since conical spin-spirals also resemble snap shots of a single magnon in a ferromagnet at a fixed time, the SSDWs introduced above are sometimes called "frozen magnons". Calculations for different (small) $\mathbf{q}$ values (e.g., using the generalized Bloch theorem) can be used to simulate the effect of temperature on a magnetic system in the adiabatic approximation. At very low temperatures, when magnons with long wavelengths dominate and no Stoner excitations are present, this is a reasonable approximation. In the long wavelength limit, i.e., around $\mathbf{q} = 0$, the spin-wave dispersion behaves almost quadratically and can be described as $E(\mathbf{q}) = Dq^2$. The spin stiffness, D, characterizes the magnetic properties of a ferromagnet at low temperatures and can be calculated from SSDW calculations directly or from the exchange coupling constants in real space. Consider e.g., the Heisenberg term of Eq. (20) in one dimension: Then

$$\delta E(\mathbf{q}) = E(\mathbf{0}) - E(\mathbf{q}) = +2M^2\sum_{\nu>0} J_{0\nu}\left(1-\cos\left(\mathbf{q}\mathbf{R}_\nu\right)\right) \approx 2M^2q^2\sum_{\nu>0} J_{0\nu}\mathbf{R}_\nu^2 \tag{23}$$

and D is obtained as $2M^2\sum_{\nu>0} J_{0\nu}\mathbf{R}_\nu^2$. In more dimensions D is a tensorial quantity and the exact expression depends on the crystal symmetry. Some results of an isotropic D obtained from DFT calculations for cubic systems are given in Table 5. For Fe and Co agreement with experimental data is reasonable, but for Ni most methods fail to reproduce the experimental spin stiffness. More about spin-waves can be found e.g., in the review of Staunton (1994) and in a following chapter. Calculations of the full magnon spectra of Fe and Ni can be found e.g., in the work of Halilov et al. (1997). The agreement with experimental spectra, even for larger $\mathbf{q}$ values is quite satisfactorily, therefore these calculations can also serve as a starting

Table 5 Calculated and experimental spin-wave stiffness (D) for Fe, Co and Ni. The theoretical values were obtained in different approximations as described by Rosengaard and Johansson (1997) [th.(1)], Kübler (2000) [th.(2)], Shallcross and coworkers (2005) [th.(3)] and Pajda et al. (2001) [th.(4)], experimental data were taken as cited in these references

D (meV Å^2)	th.(1)	th.(2)	th.(3)	th.(4)	Exp.
Fe (bcc)	247	355	322,313	250	280,314,330
Co (fcc)	502	510	480,520	663	510,580
Ni (fcc)	739	790	541,1796	756	422,550,555

point to calculate finite temperature properties, like the Curie temperature. One has to keep in mind, however, that for other systems it is not guaranteed that they can be treated in such simple model.

In the discussion of spin waves so far the influence of spin-orbit coupling was neglected. Therefore, the so obtained "spin-excitations" are always gapless while in a system with magnetic anisotropy there is an energy to overcome for a finite $\mathbf{q}$ value. Moreover, the Dzyaloshinskii-Moriya interaction leads to a finite energy difference between clockwise and anticlockwise rotating magnons (Udvardi and Szunyogh 2009).

4.2 Ordering Temperatures

Extending the description of finite-temperature magnetic properties of bulk ferromagnets to the point where transverse fluctuations finally destroy the magnetic order, here the simplest model is presented, the so-called mean field approximation (MFA). A selected site 0 experiences an effective field from all other atoms; At $T = 0$ it is proportional to $M \sum_{\nu \neq 0} J_{0\nu} = M J_0$, while at $T > 0$ this field is reduced by thermal fluctuation on the sites ν:

$$B_{\text{eff}} = \sum_{\nu} J_{0\nu} \langle M(\mathbf{R}_\nu) \rangle, \tag{24}$$

where the thermal average of the projection of the magnetization at site ν on the magnetization at site 0 is denoted as $\langle M(\mathbf{R}_\nu) \rangle$. In this model the temperature where the average magnetization vanishes (for ferromagnetic systems the Curie temperature) is given by

$$k_{\text{B}} T_{\text{C}}^{\text{MFA}} = \frac{2}{3} J_0 M^2 \eta, \tag{25}$$

where $\eta \to 1$ in the classical limit (Liechtenstein et al. 1986). In many cases the MFA overestimates T_{C} and other models, like the random phase approximation (RPA) are preferable. Moreover, in lower-dimensional systems the MFA cannot be applied, e.g., a finite the magnetic anisotropy is essential to stabilize magnetic

Table 6 Calculated and experimental Curie temperature T_C for some ferromagnetic materials. MFA[1] and RPA data for Fe, Co and Ni taken from Pajda et al. (2001), MFA[2] results and experimental values as quoted by Shallcross and coworkers (2005), while the MC results were obtained by Rosengaard and Johansson (1997). Spin dynamics (SD) calculations have been performed by Antropov (2005). Data for Gd can be found in the papers of Kurz et al. (2002) and Turek and coworkers (2003a)

T_C (K)	MFA[1]	MFA[2]	RPA	MC	SD	Exp.
Fe (bcc)	1414	550,1190	950	1060	1070	1044 – 1045
Co (fcc)	1645	1120,1350	1311	1080		1388 – 1393
Ni (fcc)	397	320,820	350	510	470	624 – 631
Gd (hcp)	334					293

order in two dimensions (Bander and Mills 1988). However relativistic DFT calculations provide the necessary ingredients to calculate also T_C in two dimensional systems (Udvardi and Szunyogh 2009). Also for antiferromagnets (or, generally spin-spiral states) expressions for the ordering temperature, the Néel temperature T_N, can be derived (Turek et al. 2003b). There exist several more methods to calculate critical temperatures from DFT results, e.g., the Monte Carlo technique (MC) allows studying finite-temperature magnetic properties by implementation of a Heisenberg Hamiltonian, possibly with extensions like the magnetic anisotropy like in Eq. (20). Some applications for multi-sublattice systems are shown in the work of Ležaić et al. (2013).

The Curie temperature of Fe, Co, Ni and Gd obtained in different approximations with parameters from DFT calculations are presented in Table 6. Compared to RPA, the MFA overestimates T_C by 25–50% in these cases. For Fe and Co RPA gives quite good estimates of the Curie temperature, while for Ni T_C is underestimated in both approximations. From Table 1 it can be seen that this behavior is not universal and for some materials the MFA results compare very well with experimental data.

MC simulations work better for Ni and Fe, but give a too low T_C for Co. Finally, the results of spin dynamics calculations, performed along the line sketched in Sect. 3.1, give results comparable to MC calculations for Fe and Ni, but have the advantage that they do not rely on a model Hamiltonian (Antropov 2005). Also in the work of Skubic et al. (2008) it can be seen that SD and MC results for bcc Fe are very similar.

5 Conclusion

Within this small chapter I tried to give an impression of the possibilities that DFT calculations can give to calculate magnetic properties of elemental magnets and some compounds, mainly focusing on bulk materials. I left out many classes of magnetic materials, e.g., transition metal oxides, where correlation effects complicate the picture and extensions like LDA + U (Anisimov et al. 1997) or LDA + DMFT (Held et al. 2002) are required to capture many aspects of their

properties. Of course, there are many more magnetic properties where DFT can be very useful for modeling, e.g., the coupling of electrons with the nuclear spin that has been neglected here. Nevertheless, I hope that this chapter gives at least a staring point to explore the power of ab initio methods to model magnetic systems.

References

Anisimov VI, Aryasetiawan F, Lichtenstein AI (1997) First-principles calculations of the electronic structure and spectra of strongly correlated systems: the LSDA+U method. J Phys Condens Matter 9:767–808

Antropov V (2005) Magnetic short-range order above the Curie temperature of Fe and Ni. Phys Rev B 72:140406

Antropov VP, Katsnelson MI, van Schilfgaarde M, Harmon BN (1995) Ab initio spin dynamics in magnets. Phys Rev Lett 75:729–732

Antropov VP, Katsnelson MI, Harmon BN, van Schilfgaarde M, Kusnezov D (1996) Spin dynamics in magnets: equation of motion and finite temperature effects. Phys Rev B 54: 1019–1035

Bander M, Mills DL (1988) Ferromagnetism of ultrathin films. Phys Rev B 38:12015–12018

Beiden SV, Temmerman WM, Szotek Z, Gehring GA, Stocks GM, Wang Y, Nicholson DMC, Shelton WA, Ebert H (1998) Real-space approach to the calculation of magnetocrystalline anisotropy in metals. Phys Rev B 57:14247–14253

Bethe HA, Salpeter EE (1977) Quantum mechanics of one- and two-electron systems. Plenum, New York

Bode M, Heide M, von Bergmann K, Ferriani P, Heinze S, Bihlmayer G, Kubetzka A, Pietzsch O, Blügel S, Wiesendanger R (2007) Chiral magnetic order at surfaces driven by inversion asymmetry. Nature 447:190

Bruno P (1989) Tight-binding approach to the orbital magnetic moment and magnetocrystalline anisotropy of transition-metal monolayers. Phys Rev B 39:865–868

Bychkov YA, Rashba EI (1984) Properties of a 2D electron gas with lifted spectral degeneracy. JETP Lett 39:78–81

Dederichs PH, Blügel S, Zeller R, Akai H (1984) Ground states of constrained systems: application to cerium impurities. Phys Rev Lett 53:2512–2515

Di Napoli S, Llois AM, Bihlmayer G, Blügel S, Alouani M, Dreyssé H (2004) Magnetic structure and transport properties of noncollinear $LaMn_2X_2$ (X = Ge, Si) systems. Phys Rev B 70:174418

Dirac PAM (1930) Note on exchange phenomena in the Thomas–Fermi atom. Proc Camb Philos Soc 26:376–385

Dupé B, Bihlmayer G, Böttcher M, Blügel S, Heinze S (2016) Engineering skyrmions in transition-metal multilayers for spintronics. Nat Commun 7:11779

Dzialoshinskii IE (1957) Thermodynamic theory of "weak" ferromagnetism in antiferromagnetic substances. Sov Phys JETP 5:1259

Eich FG, Gross EKU (2013) Transverse spin-gradient functional for noncollinear spin-density-functional theory. Phys Rev Lett 111:156401/1–5

Ferriani P, Turek I, Heinze S, Bihlmayer G, Blügel S (2007) Magnetic phase control in monolayer films by substrate tuning. Phys Rev Lett 99:187203

Friesner RA (2005) Ab initio quantum chemistry: methodology and applications. PNAS 102: 6648–6653

Galler A, Taranto C, Wallerberger M, Kaltak M, Kresse G, Sangiovanni G, Toschi A, Held K (2015) Screened moments and absence of ferromagnetism in FeAl. Phys Rev B 92:205132

Halilov SV, Perlov AY, Oppeneer PM, Eschrig H (1997) Magnon spectrum and related finite-temperature magnetic properties: a first-principle approach. Europhys Lett 39:91

Halilov SV, Perlov AY, Oppeneer PM, Yaresko AN, Antonov VN (1998) Magnetocrystalline anisotropy energy in cubic Fe, Co, and Ni: applicability of local-spin-density theory reexamined. Phys Rev B 57:9557–9560

Heide M, Bihlmayer G, Blügel S (2009) Describing Dzyaloshinskii-Moriya spirals from first principles. Physica B 404:2678

Held K, Anisimov VI, Nekrasov IA, Eyert V, Keller G, Pruschke T, Vollhardt D, Blümer N, McMahan AK, Scalettar RT (2002) The LDA+DMFT approach to materials with strong electronic correlations. In: Grotendorst J, Marx D, Muramatsu A (eds) Quantum simulations of complex many-body systems: from theory to algorithms, Research Center Jülich. NIC series, vol 10. John von Neumann Institute for Computing, Jülich, pp 175–209

Herring C (1966) Exchange interactions among intinerant electrons. In: Rado GT, Suhl H (eds) Magnetism, vol IV. Academic, New York/London

Hohenberg P, Kohn W (1964) Inhomogeneous electron gas. Phys Rev 136:B864–B871

Ibañez Azpiroz J, dos Santos Dias M, Blügel S, Lounis S (2016) Zero-point spin-fluctuations of single adatoms. Nano Lett 16:4305–4311

Jones RO (2015) Density functional theory: its origins, rise to prominence, and future. Rev Mod Phys 87:897–923

Kohn W, Sham L (1965) Self-consistent equations including exchange and correlation effects. Phys Rev 140:A1133–A1138

Kokalj A (2003) Computer graphics and graphical user interfaces as tools in simulations of matter at the atomic scale. Comput Mater Sci 28:155–168

Koller D, Tran F, Blaha P (2011) Merits and limits of the modified Becke-Johnson exchange potential. Phys Rev B 83:195134/1–10

Kota Y, Sakuma A (2014) Mechanism of uniaxial magnetocrystalline anisotropy in transition metal alloys. J Phys Soc Jpn 83(3):034715

Kübler J (2000) Theory of itinerant electron magnetism. International series of monographs in physics, vol 106. Clarendon Press, Oxford

Kurz P, Bihlmayer G, Blügel (2002) Magnetism and electronic structure of hcp Gd and the Gd(0001) surface. J Phys Condens Matter 14:6353–6371

Kurz P, Förster F, Nordström L, Bihlmayer G, Blügel S (2004) Ab initio treatment of non-collinear magnets with the full-potential linearized augmented planewave method. Phys Rev B 69:024415/1–15

Ležaić M, Mavropoulos P, Bihlmayer G, Blügel S (2013) Exchange interactions and local-moment fluctuation corrections in ferromagnets at finite temperatures based on noncollinear density-functional calculations. Phys Rev B 88:134403

Liechtenstein AI, Katsnelson MI, Antropov VP, Gubanov VA (1986) Local spin density functional approach to the theory of exchange interactions in ferromagnetic metals and alloys. J Magn Magn Mater 67:65–74

Millhouse AH, McEwen KA (1973) Neutron diffraction study of single crystal europium in an applied magnetic field. Solid State Commun 13:339–345

Młyńczak E, Eschbach M, Borek S, Minár J, Braun J, Aguilera I, Bihlmayer G, Döring S, Gehlmann M, Gospodarič P, Suga S, Plucinski L, Blügel S, Ebert H, Schneider CM (2016) Fermi surface manipulation by external magnetic field demonstrated for a prototypical ferromagnet. Phys Rev X 6:041048

Moriya T (1960) Anisotropic superexchange interaction and weak ferromagnetism. Phys Rev 120:91–98

Moruzzi VL, Janak JF, Williams AR (1978) Calculated electronic properties of metals. Pergamon, New York

Moruzzi VL, Marcus PM, Schwarz K, Mohn P (1986) Ferromagnetic phases of bcc and fcc Fe, Co, and Ni. Phys Rev B 34:1784–1791

Pajda M, Kudrnovský J, Turek I, Drchal V, Bruno P (2001) Ab initio calculations of exchange interactions, spin-wave stiffness constants, and Curie temperatures of Fe, Co, and Ni. Phys Rev B 64:174402

Pickard CJ, Mauri F (2001) All-electron magnetic response with pseudopotentials: NMR chemical shifts. Phys Rev B 63:245101/1–13

Ravindran P, Kjekshus A, Fjellvåg H, James P, Nordström L, Johansson B, Eriksson O (2001) Large magnetocrystalline anisotropy in bilayer transition metal phases from first-principles full-potential calculations. Phys Rev B 63:144409

Rosengaard NM, Johansson B (1997) Finite-temperature study of itinerant ferromagnetism in Fe, Co, and Ni. Phys Rev B 55:14975–14986

Sandratskii LM (1991) Symmetry analysis of electronic states for crystals with spiral magnetic order. I. General properties. J Phys Condens Matter 3:8565

Schweflinghaus B, Zimmermann B, Heide M, Bihlmayer G, Blügel S (2016) Role of Dzyaloshinskii-Moriya interaction for magnetism in transition-metal chains at Pt step edges. Phys Rev B 94:024403

Shallcross S, Kissavos AE, Meded V, Ruban AV (2005) An ab initio effective Hamiltonian for magnetism including longitudinal spin fluctuations. Phys Rev B 72:104437/1–8

Shick AB, Mryasov ON (2003) Coulomb correlations and magnetic anisotropy in ordered $L1_0$ CoPt and FePt alloys. Phys Rev B 67:172407

Singh DJ, Ashkenazi J (1992) Magnetism with generalized-gradient-approximation density functionals. Phys Rev B 46:11570–11577

Skubic B, Hellsvik J, Nordström L, Eriksson O (2008) A method for atomistic spin dynamics simulations: implementation and examples. J Phys Condens Matter 20(31):315203

Slater JC (1951) A simplification of the Hartree-Fock method. Phys Rev 81:385–390

Staunton JB (1994) Electronic structure of magnetic transition metallic materials. Rep Prog Phys 57:1289–1344

Thoene J, Chadov S, Fecher G, Felser C, Kübler J (2009) Exchange energies, Curie temperatures and magnons in Heusler compounds. J Phys D Appl Phys 43:084013

Thonhauser T, Ceresoli D, Vanderbilt D, Resta R (2005) Orbital magnetization in periodic insulators. Phys Rev Lett 95:137205/1–4

Trygg J, Johansson B, Eriksson O, Wills JM (1995) Total energy calculation of the magnetocrystalline anisotropy energy in the ferromagnetic 3*d* metals. Phys Rev Lett 75:2871–2874

Turek I, Kudrnovský J, Bihlmayer G, Blügel S (2003a) Ab initio theory of exchange interactions and the Curie temperature of bulk Gd. J Phys Condens Matter 15(17):2771

Turek I, Kudrnovský J, Diviš M, Franek P, Bihlmayer G, Blügel S (2003b) First-principles study of the electronic structure and exchange interactions in bcc europium. Phys Rev B 68:224431

Udvardi L, Szunyogh L (2009) Chiral asymmetry of the spin-wave spectra in ultrathin magnetic films. Phys Rev Lett 102:207204

van der Laan G (1998) Microscopic origin of magnetocrystalline anisotropy in transition metal thin films. J Phys Condens Matter 10(14):3239

von Barth U, Hedin L (1972) A local exchange-correlation potential for the spin polarized case: I. J Phys C Solid State Phys 5:1629–1642

Weinert M, Watson RE, Davenport JW (1985) Total-energy differences and eigenvalue sums. Phys Rev B 32:2115–2119

White HW, Beaudry BJ, Burgardt P, Legvold S, Harmon BN (1975) Magnetic moments of ferromagnetic gadolinium alloys. AIP Conf Proc 29:329

Yang I, Savrasov SY, Kotliar G (2001) Importance of correlation effects on magnetic anisotropy in Fe and Ni. Phys Rev Lett 87:216405/1–4

Yosida K (1996) Theory of magnetism. Springer, Berlin/Heidelberg